SCALING DOWN HALL THRUSTERS

E. Ahedo and J.M. Gallardo

E.T.S.I. Aeronáuticos, Universidad Politécnica de Madrid, Spain

IEPC-2003-104

Abstract

Hall thrusters in the 50-100W range with good performances in terms of efficiency, specific impulse, and lifetime remain today a technical challenge. The main laws governing the plasma discharge and the critical technical issues for these low-power thrusters are summarized. based on them, two design strategies are proposed to scale down existing 500-1000W prototypes to the 50W case. A pre-design exercise based on one of these strategies is carried out.

1 Introduction

Due to different technical and economical reasons, the interest on small-satellite programs has increased significantly in the last ten years. Different electric propulsion devices are being considered as thruster options for mini-spacecraft. In particular, Hall thrusters(HT) are potential candidates for the 50-500W range [1]. Table 1 presents a (non exhaustive) list of classical and recent prototypes within that range. The list starts with the well-known SPT-50, and continues with other five Russians designs of the SPT-type. The US BHT-200 presents some innovations within the ceramic-wall type and is one of the propulsion systems selected for the TechSat-21 program of the USAF [2]. Table 1 continues with two Russian TAL designs, and ends with the most challenging prototype, the MIT 50W thruster [3]. The comparison of the different thrusters show a steady decrease of their performances as their nominal power is reduced. Down to 200W of nominal power, Hall thrusters present competitive capabilities, with (anode) efficiencies above 25% and specific impulses about 1500s. Performances deteriorate rapidly in the 100W range. Finally, the MIT 50W thruster had an unexpected bad behavior, possibly because of an error in the magnetic circuit design.

Therefore, we can set the current development objective in low power HT as a 50-100W design with performances comparable to 200W models. As a contribution to that effort, here, we start summarizing the main characteristics of the plasma discharge and the resulting scaling laws for the main parameters governing the discharge. Then, we review briefly the technical constraints for low power thrusters. Finally, based on both the discharge physics and the critical technical issues we compare two different scaling strategies for a low-power design. The discussion is centered on the SPT-class of thrusters.

2 Plasma discharge characteristics

The usual design procedure is based on scaling down the parameters characterizing existing mid-power thrusters. The design will try to preserve the fundamental properties of the plasma discharge and, at the same time, to solve adequately the main technical issues affecting the thruster performance and integrity.

The plasma response depends on several thruster parameters related to

- thruster operation: discharge voltage V_d, (anode) mass flow $\dot{m}_A$, magnetic field $B(\boldsymbol{r})$.
- geometry of the discharge chamber: length L_c, mid-radius r_c, and width h_c.
- wall material properties: SEE yield δ_w, and erosion rate.

From our present understanding of the discharge physics in the HT chamber, the discharge is characterized by the following properties [4, 5].

- The plasma Debye length λ_D is much smaller than any geometrical length. Thus, the plasma is quasineutral in the bulk of the chamber and space-charge electric fields are limited to Debye sheaths around the lateral and rear walls. For a typical discharge $\lambda_D \sim 10^{-2} - 10^{-1}$mm, so the quasineutrality condition is easily satisfied even for small-size HT (which, in addition, tend to operate with smaller λ_D).

- Large discharge voltages are desirable to attain large specific impulses, $I_{sp}(\propto V_d^{1/2})$, but lead to larger erosion rates and thermal loads. Thus, low-power designs tend to decrease V_d to limit that problems. The lower bound of V_d is set mainly by high-ionization considerations. The maximum plasma temperature $T_{e,max}$ in the chamber should be higher than 12-15eV to facilitate a short and efficient ionization region. $T_{e,max}$ is determined from the balance of Joule heating (proportional to V_d, roughly), wall losses (which depend on the SEE yields and the electron distribution function) and ionization losses. We estimate the lower bound of V_d to be around 75V for an efficient ionization.

- Normally, the axial profile of the radial magnetic field, $B(x)$, presents a large gradient with the maximum field, B_{max}, near the channel exit. Two reasons are invoked for it: the stability of the discharge and a higher efficiency [6].

- With respect to the magnetic field strength, B_{max}, the first condition is to force the main electron population to follow a quasi-closed $E \times B$ drift. This requires that

$$L_c \gg \ell_e \propto B_{max}^{-1}, \quad \nu_e \ll \omega_e \propto B_{max}, \tag{1}$$

  where ν_e is the effective axial diffusion frequency of electrons. The dominant contribution to ν_e is not clearly identified yet: fluctuation-based diffusion and wall collisionality are the most plausible candidates. In the first case, experimental data suggest $\nu_e \propto \alpha_{ano}\omega_e$ with $\alpha_{ano} \sim 0.01 - 0.1$. In the second case, one has $\nu_e/\omega_e \sim \beta_m \nu_w$, with ν_w a typical frequency for plasma recombination at the lateral walls and $\beta_m \sim 0 - 100$ depending on the electron collisional process with the wall.

- Then, for each V_d, the *optimum operation* value of B_{max} is set in order to maximize the thrust efficiency and to generate a low-oscillatory discharge. The optimum B_{max} increases with V_d at a rate that depends on the thruster design and its operation range. (In all cases, the resulting B_{max} is such that the ion motion is practically unmagnetized, $L_c \ll \ell_i$.)

- For an SPT-type thruster, the chamber length, L_c, must be large enough to accommodate the ionization and acceleration regions of the discharge. In a high-efficiency regime, the internal structure usually includes an ion reverse-flow region between the anode and the ionization region [7, 8]. The value of the chamber width, h_c, is a trade-off between low values (appropriate for a 1D plasma acceleration and a better configuration of the B-field) and large values (convenient to minimize wall losses).

The plasma discharge model of Refs. [5, 9] propose expressions for several of the main scaling laws of the discharge, which we summarize here.

- The length of the ion-backstreaming and ionization regions follows $L_{b+i} \sim \sqrt{\nu_e/\nu_{ion}}\,\ell_e$. If turbulent diffusion dominates, we better write $L_{b+i} \sim c_e\sqrt{\alpha_{ano}/\nu_{ion}\omega_e}$, where we see that L_{b+i} increases when $B(x)$ decreases (in the rear part of the chamber). The typical plasma density in that region is $n_e \sim \dot{m}_A/(m_i \nu_{ion} \times L_{b+i} r_c h_c)$. The voltage drop in that region is $V_{b+i} < T_{e,max}/2 \ll V_d$, so most of the voltage drop takes place in the internal and external acceleration regions.

- The analysis of the acceleration regions yields

$$V_d^{1/2} \propto \frac{I_{dr}}{I_{i\infty}} \times \frac{B_{max}}{\alpha_{ano}} \times L_{acc}, \tag{2}$$

which is one of the main scaling laws of the discharge. Here, $I_{dr} = I_d - I_{i\infty}$ is the incoming electron current, $L_{acc} = L_c + L_{cat} - L_{b+i}$ is the length of the acceleration region, and L_{cat} the distance, from the chamber exhaust, of the effective beam-neutralization surface. Therefore, as B_x is (uniformly) increased, L_{b+i} decreases, L_{acc} increases, and V_d increases too.

- The details of the *optimum operation* law for $V_d(B_{max})$ depend on the behavior of $I_{dr}/I_{i\infty}$ in Eq. (2). The plasma energy balance shows that $I_{dr}/I_{i\infty} \sim P_{loss}/P_d$, where the power loss $P_{loss} = P_{anode} + P_{ion} + P_{wall}$ includes contributions from anode heating, ionization and interaction with the lateral walls. For long chambers and high voltages the last component is the dominant one and satisfies $P_{wall} \sim \nu_w \beta_e n_e T_{e,max} r_c h_c L_c$, where $\nu_w \propto h_c^{-1}\sqrt{T_e/m_i}$ is the plasma recombination frequency and β_e an energy-loss factor which depends on the SEE behavior.

2.1 Universal class of solutions

Let us keep $V_d = \text{const}$ and vary the anode mass flow $\dot{m}_A$. Then, the dis that a universal class of solutions of the discharge is defined by the following scaling laws:

$$V_d = \text{const}, \qquad \dot{m}_A, h_c, r_c, L_c \propto P_d, \qquad B_{max} \propto P_d^{-1}, \tag{3}$$

for the input variables, and

$$I_{sp}, \eta = \text{const}, \qquad F, I_d, P_{ion}, P_{wall} \propto P_d, \tag{4}$$

for the output ones.

3 Technical constraints

The behavior of a HT does not depend only of an optimum plasma discharge. The main technical issues affecting the thruster design are commented now.

3.1 Erosion

Total erosion of the ceramic walls is the main factor limiting the HT lifetime. Two different processes have been identified: classical ion sputtering and anomalous erosion [10]. The mechanism of the second one is bad known. We focus here on ion sputtering. The rate of erosion of the insulator wall can be written as

$$\frac{d}{dt}(\delta h_{ins}) = -g_{ri}\frac{Y(\epsilon,\theta)}{n_{ins}} \quad \Longrightarrow \quad t_{life} \sim \frac{h_{ins}}{n_e T_e^{1/2}} < \frac{n_{ins}}{Y(\epsilon,\theta)} >, \tag{5}$$

with n_{ins} and h_{ins} the insulator density and (initial) thickness, $\delta h_{ins}(t)$ the instantaneous thickness, g_{ri} the radial ion flux to the wall, and $Y(\epsilon,\theta)$ the sputtering function, in units of sputtered particles per incident ion. This function depends on the ion energy ($\epsilon \sim \frac{1}{2} m_i \boldsymbol{v}_i^2 \sim eV_d$) and the incidence angle θ. Angles about $\theta \sim 60^o$ seem to be the worse, but the data published on Y is insufficient to carry out reliable estimates. A typical value for BN materials (and nominal conditions of a mid-power SPT) would be 5μm/h, which we will use to estimate crudely $< Y(\epsilon,\theta)/n_{ins} >$ and the lifetime for $V_d \sim 300V$. The variation of Y with ϵ must be taken into account for other discharge voltages.

3.2 Magnetic circuit

This is the second critical aspect for small thruster designs [3, 11]. The identified problems are

- Asymmetries, defocusing, non-uniformity of the magnetic field profile in the chamber, which penalize the efficiency and might increase the erosion rate and local thermal loads.
- Saturation of the magnetic material.
- Demagnetization, due to overheating.

These constraints become worse as the design value of B_{max} increases.

Except the MIT-50W thruster, which uses permanent magnets to create the B-field, the rest of available prototypes use coils wrapped around a ferromagnetic material. These coils dissipate a power P_{mag} which can be significant in low-power designs. Thus, P_{mag} must be computed for both the total thermal load and the total electric power required by the thruster. If the magnetic field follows $B \simeq \mu_0 NI/h_c$, with N the number of turns of the coils and I the current on the circuit, the magnetic power satisfies

$$P_{mag} = \rho_w \frac{l_w}{\pi r_w^2} \Big(\frac{h_c B}{\mu_0 N}\Big)^2 = \frac{8\rho_w}{\mu_o^2} \frac{r_s}{h_s L_s} h_c^2 B^2 \;\propto\; \frac{h_c^2 B^2}{L_s}, \tag{6}$$

with ρ_w the wire resistivity, l_w and r_w the wire dimensions and L_s, r_s, and h_s, representing the geometrical dimensions of the whole coil.

3.3 Thermal loads

The main heat sources on a HT are P_{mag} and the heat deposited at the chamber walls and the anode, P_{wall} and P_{anode}. A detailed thermal characterization of the thruster depends on geometrical aspects and material properties. For scaling purposes we are interested mainly in an estimate of the thruster maximum temperature, T_t, in terms of the different thermal loads. Thus, if the heat deposition per unit of transversal area of the thruster follows $\sim P_{heat}/L_t^2$ with $P_{heat} = P_{wall} + P_{anode} + P_{mag}$ and L_t the thruster typical length (which, by the way, is generally much larger than the chamber length, $L_t \gg L_c$), the conductive and radiative cooling rates per unit of area follow $\sim K_t T_t/L_t$ and $\sim \epsilon_r(T_t)\sigma_r T_t^4$, respectively. Then, the temperature gradients follows one of the scaling laws

$$T_t \propto \frac{P_{heat}}{K_t L_t}, \qquad T_t \propto \Big(\frac{P_{heat}}{\epsilon_r \sigma_r L_t^2}\Big)^{1/4}. \tag{7}$$

3.4 Other considerations

Low-power HT require specific developments of small cathodes for beam neutralization. The main requirements for these devices are very low power consumption and mass flows for not penalizing the thruster efficiency. A contribution below 10% of the total gas and power consumption can be an initial objective. Recent developments of low-power hollow-cathodes are: a KeRC cathode with 0.05-0.1 mg/s, 10 W, and no heater [12]; and a Busek cathode of 0.08 mg/s, 700 mA, no heater, and no keeper in the stationary mode [11]. These flow rates are still large for a 50-100W thruster. In addition to the impact on efficiency, the impact on the plume of the cathode mass flow must be evaluated too. The FEA technology, when fully developed, could be a better alternative.

Spacecraft/plume interaction is another issue to be addressed. As a general rule, low V_d or shorter chambers yield a less supersonic beam and a larger plume divergence.

The manufacturability and assembly tolerances of the small pieces of a 50W thruster can be both a practical and an economical problem [3, 1].

Finally, the design of low-power HT of the TAL-type presents similar issues [13]. Within the advantages of TAL-designs we note (i) lower energy losses at the walls and (ii) a larger

lifetime, whereas the likely disadvantages are (i) larger boundary effects and sensitivity to misalignment, (ii) non optimal B profile, (ii) larger B-field, and (iv) larger plume divergence [3].

4 Design strategies

4.1 Ideal scaling

It is based on the universal class of solutions studied previously, and its main appeal is to keep constant (and presumably maximum) the thrust efficiency. However, the resulting design presents severe problems of fabrication and operation. These difficulties come mainly from the large magnetic field and the high plasma density, both scaling as P_d^{-1}.

The ideal scaling was proposed by Khayms and Martínez-Sánchez and applied to the design of the MIT-50W thruster. This a TAL-type thruster made with permanent magnets, which were designed to create a 5000G magnetic field. A SmCo alloy was used, which, in addition, could withstand large operating temperatures without demagnetization.

To quantify the technical constraints that accompany an ideal scaling, we assume that the geometrical size of the thruster scales as $L_t \propto P_d^{1/3}$, in order that the ratio (thruster mass)$/P_d$ remains constant. Notice that we have $L_c \propto P_d$, so that the relative size of the discharge chamber, L_c/L_t, decreases with the thruster size. For the insulator thickness, the choice is between two extreme cases: $h_{ins} \propto r_t \propto P_d^{1/3}$ and $h_{ins} \propto r_c \propto P_d$. The first one would be desirable, but a correct focusing of the B-field might force to use the last one. The first one is used for the computations here. Then, we have the following scaling laws and behavior (for P_d decreasing):

- Reduction of lifetime: $t_{life} \propto P_d^{4/3}$.
- Increase of the thruster temperatures: $T_t \propto P_d^{-2/3}$.
- Penalty on the overall thruster efficiency (when coiled are used): $P_{mag}/P_d \propto P_d^{-4/3}$.

(P_{mag} is not included in the usual definition of the thrust efficiency, which is based exclusively on the discharge conditions.)

4.2 Radial scaling

The central idea of the radial scaling is to modify as less as possible the plasma conditions (density and temperature) inside the thruster chamber. As in the ideal scaling, the first decisions are to keep fixed the discharge voltage and to modify the discharge power through the control of the gas flow. Second, the axial length of the chamber and the magnetic field profile remain fixed too, whereas the radial magnitudes are changed in order to preserve the plasma density.

The scaling laws for the discharge variables are the following. Input parameters follow

$$V_d, B_{max}, L_c = \text{const}, \qquad \dot{m}_A \propto P_d, \qquad h_c, r_c \propto P_d^{1/2}, \tag{8}$$

and output parameters evolve approximately as

$$n_e, I_{sp}, L_{b+i} \propto \text{const}, \quad P_{wall} \propto P_d^{1/2}, \quad I_d, F, P_{ion} \propto P_d. \tag{9}$$

As long as P_{wall} dominates the energy losses, the thrust inefficiency behaves as

$$1 - \eta \sim \epsilon_{wall} = P_{wall}/P_d \propto P_d^{-1/2}. \tag{10}$$

Therefore, the main disadvantage of this scaling for down-sizing is an increasing penalty on the thrust efficiency.

This drawback is compensated by milder technical constraints than the ideal scaling. Selecting the rest of thruster magnitudes as in the previous strategy, the other relevant scaling laws are

- Lifetime: $t_{life} \propto P_d^{1/3}$.
- Thruster temperature: $T_t \propto P_d^{-1/6}$.
- Efficiency penalty from the magnetic circuit: $P_{mag}/P_d \propto P_d^{-5/6}$.

To minimize the loss of thrust efficiency, Eq. (10), the second stage of this scaling strategy would be to optimize η by adjusting the pairs of parameters (L_c, B_{max}) and $(V_d, \dot{m}_A)$.

The data of Table 1 and of the complete SPT series suggests that a strategy similar to this radial scaling has been followed on the design of most prototypes.

4.2.1 Predesign of a mini HT

As a testing of the radial scaling strategy we used the axial model of Ref. [5] and the rest of performance laws derived above to design a 45W thruster, departing from the nominal values of the SPT-50, shown in Table 1. Figure 1 shows the axial profile of the selected 'nominal' case for the SPT-50; the wall material was selected such that a 100% SEE yield takes place for $T_e \simeq 40$eV. Relevant output magnitudes are $\eta = 40\%$ and $I_{sp} = 1550s$.

Figure 2 shows the scaling down of the thruster from 300W to 45W, following the radial scaling except that B_{max} is not kept constant, but tuned slightly in order that the discharge corresponds always to *optimum operation*. Figure 3 depicts the axial profile for the resulting 45W thruster. Notice the similarity of the profiles of all magnitudes with the 300W thruster of Fig. 1.

Figure 4 and 5 illustrate the second stage of the design, when some parameters are modified in the search of better performances. In both cases, B_{max} is tuned to keep optimum operation. Figure 4 shows that the variation of (L_c, B_{max}) has no impact on η, but larger lifetimes and specific impulses are obtained for larger chambers; notice that $B_{max} \propto L_c^{-1}$, as expected.

In Figure 5, V_d, $\dot{m}$, and B_{max} are changed in the following way: the mass flow satisfies $\dot{m} \propto V_d^{-1}$, and B_{max} is set for optimum operation. Notice that, in this procedure, $P_d = I_d V_d$ changes with the inverse of the discharge efficiency, $\eta_d = e\dot{m}/m_i I_d$. The results show a better behavior for low V_d, but this improvement is due partially to a higher P_d.

5 Conclusions

The basic characteristics of the plasma discharge can be preserved in Hall thrusters of 50-100W, so the discharge does not pose big difficulties in the design of low-power HT. The fundamental obstacles for these thrusters lie in (i) the design of the magnetic circuit (to avoid saturation and to obtain the correct shape and focusing) (ii) the overheating (with the risk of demagnetization) (iii) a strong reduction of the lifetime, and (iv) a correct manufacturing and assembly. Thus, research should focus on a careful study of the magnetic circuit, the heat evacuation paths, an easy-to-manufacture design, and the selection of appropriate materials.

Two design strategies have been discussed here. The ideal scaling is the most ambitious one in terms of thrust efficiency and scientific-technical challenge. The radial scaling proposes a compromise among the main practical requirements. In the second case, 50W designs with $\eta > 20\%$, $I_{sp} > 1000$s, and $t_{life} > 1000$h seem achievable.

Acknowledgments

The participation of the authors was financed by Alta/ESA (for E.A.) and the European Office for Aerospace Research and Development, under Contract F61775-01-WE070 (for J.M.G.).

References

[1] M.M. Micci and A.D. Ketsdever, editors. *Micropropulsion for small spacecraft.* AIAA, Washington, DC, 2000.

[2] R.A. Spores and M. Birkan. AIAA 2002-3558, 2002.

[3] V. Khayms and M. Martínez-Sánchez. In Ref. 1, chapter 9.

[4] E. Ahedo, J.M. Gallardo, and M. Martínez-Sánchez. AIAA 2002-4244, 2002.

[5] E. Ahedo, J.M. Gallardo, and M. Martínez-Sánchez. *Submitted to Phys. Plasmas*, 2003.

[6] V.V. Zhurin, H.R. Kaufman, and R.S. Robinson. *Plasma Sources Sci. Technol.*, 8:R1–R20, 1999.

[7] A.M. Bishaev and V. Kim. *Sov. Physics-Tech. Physics*, 23(9):1055–1057, 1978.

[8] E. Ahedo, J.M. Gallardo, and M. Martínez-Sánchez. *Phys. Plasmas*, 9(9):4061–4070, 2002.

[9] E. Ahedo, J.M. Gallardo, F.I. Parra, and C. Pérez Trigo. IEPC-2003-331, 2003.

[10] A.I Morozov and V.V. Savelyev. *Reviews of Plasma Physics*, volume 21, chapter 2. Kluwer Academic, New York, 2000.

[11] J. Monheiser, V. Hruby, C. Freeman, W. Connolly, and B. Pote. In Ref. 1, chapter 10.

[12] O.A. Gorshkov and etal. AIAA-2001-3229, 2001.

[13] L. Zakharenkov, G. Chislov, A. Semenkin, and T. Lawrence. IEPC-01-041, 2001.

[14] D.H. Manzella, S. Oleson, J. Sankovic, T. Haag, A. Semenkin, and V. Kim. AIAA-96-2736, 1996.

[15] G. Guerrini, C. Michaut, M. Dudeck, A.N. Vesselovzorov, and M. Bacal. IEPC 97-053, 1997.

[16] B. Arkhipov, A. Bober, M. Day, R. Gnizdor, K. Kozubsky, and N. Maslennikov. AIAA-96-2708, 1996.

[17] M.B. Belikov, O.A. Gorshkov, V.A. Muravlev, R.N. Rizakhanov, A.A. Shagayda, and A.U. Shnirev. AIAA-2001-3780, 2001.

[18] M.B. Belikov, O.A. Gorshkov, and R.N. Rizakhanov. IEPC-99-094, 1999.

[19] M.B. Belikov, O.A. Gorshkov, A.B. Jakupov, and S.A. Khartov. AIAA-98-3786, 1998.

[20] D.T. Jacobson and R.S. Jankovsky. AIAA-98-3792, 1998.

[21] B. Arkhipov and etal.. In *SP-465: 3rd Spacecraft Propulsion Conference, Cannes(Francia)*, pages 399–401, ESA, Noordwijk, The Netherlands, 2000.

model	W_d	V_d	$\dot{m}_A$	F	I_{sp}	η_A	η	other data	Ref.
SPT-50	310	280	1.26	18	1450	.42	.32	0.9kg, 1500h	[14]
	138	282	.68	8	1100	.34	.29	h_c=11mm	[14]
	110		.6	8			.18	170gauss	[15]
	86	201	.51	5.3	850	.32	.21		[14]
	47	135	.3	3.2	950			2500h	[16]
KM-37	200	270	.8	11.7	1405		.40	.05mg/s, 9W(mag), 14W(cat)	[17]
	150	236	.7	8.7	1180		.34		[17]
	100	192	.6	5.7	895		.24		[17]
KM-32	160	168	.74	10.4	1410	.45		r_c=16mm, h_c=8mm	[18]
X-40	189	320	.50	8.5	1700	.38			[19]
	110	200	.50	5.8	1160	.31		300G	[19]
SPT-30	202	200	.98	11.3	1170	.32	.29	.11mg/s(cat)	[20]
	90	150	.61	4.9	819	.22	.19	.10mg/s(cat)	[20]
SPT-25	134	180	.59	5.5	948	.22	.18		[21]
	59	100	.59	3.2	554	.17	.14	1W(mag), .07mg/s(cat)	[21]
BHT-200	200	300	.7	11.4	1500	.41	.35	0.9kg, .08mg/s	[11]
	100	192	.35	3.8	1100	.20	.15	L_c=7mm, h_c= 9.5mm	[11]
D-38	212	95	2.23	12.9	700	.21			[13]
	220	250	.88	11.4	1336	.33			[13]
	110	200	.62	5.1	862	.19			[13]
T-27	201	251	.70	9.6	1430	.33			[13]
	114	190	.53	5.3	1033	.23			[13]
MIT	100	250	.21	1.6	773		.063	L_c =1.3mm, h_c=1.6mm, 5000G	[3]
	42	200	.17	.85	515		.050	η_u=.30-.40	[3]

Table 1.- Low power prototypes.

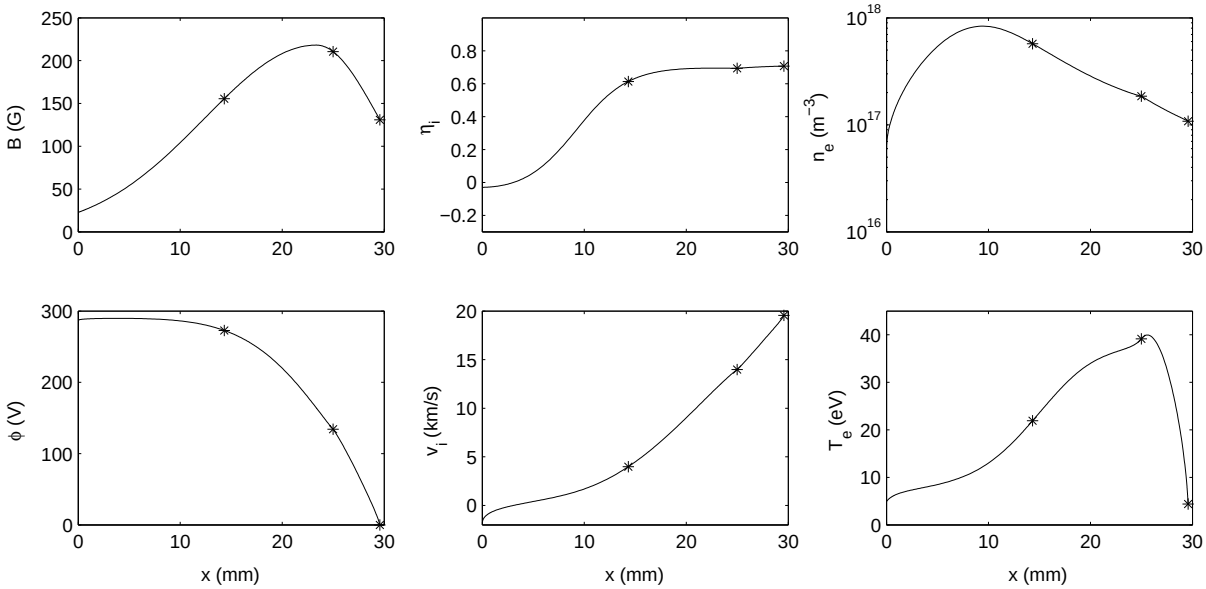

Fig. 1.- Axial profiles for the SPT-50, for $V_d = 300V$, $\dot{m}_A = 1.15$mg/s, $L_c = 25$mm, and the magnetic field profile shown in the first subplot. The nominal discharge power is 300W.

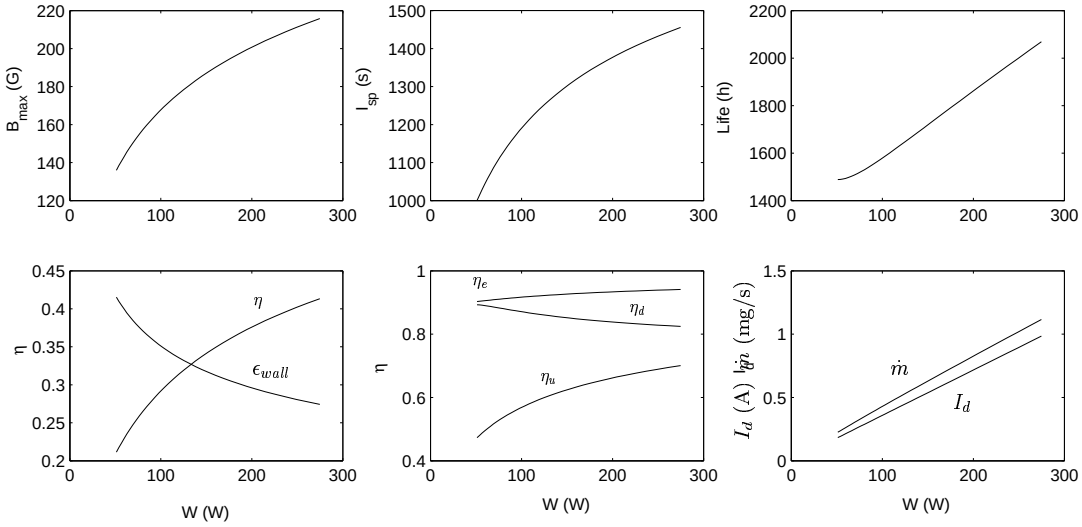

Fig. 2.- Radial scaling (except for B_{max}) from 300W to 50W; $V_d = 300$V, $L_c = 25$mm, $h_c, r_c \propto \dot{m}^{1/2}$.

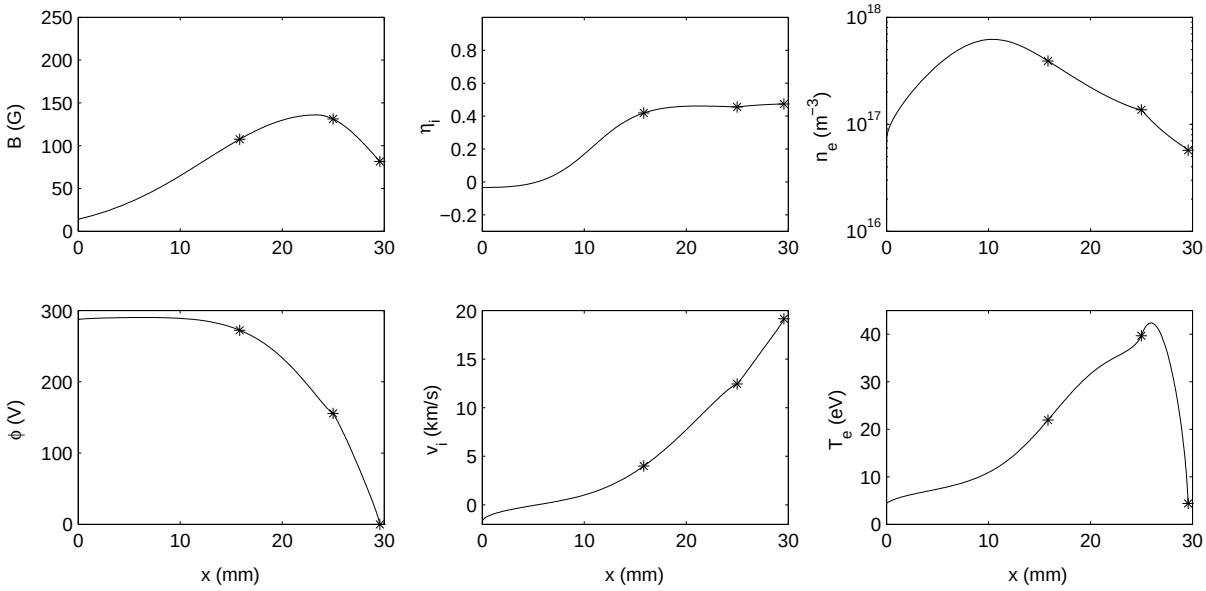

Fig. 3.- Axial profiles for the 45W thruster; $V_d = 300V$ and $\dot{m}_A = 1.15$mg/s.

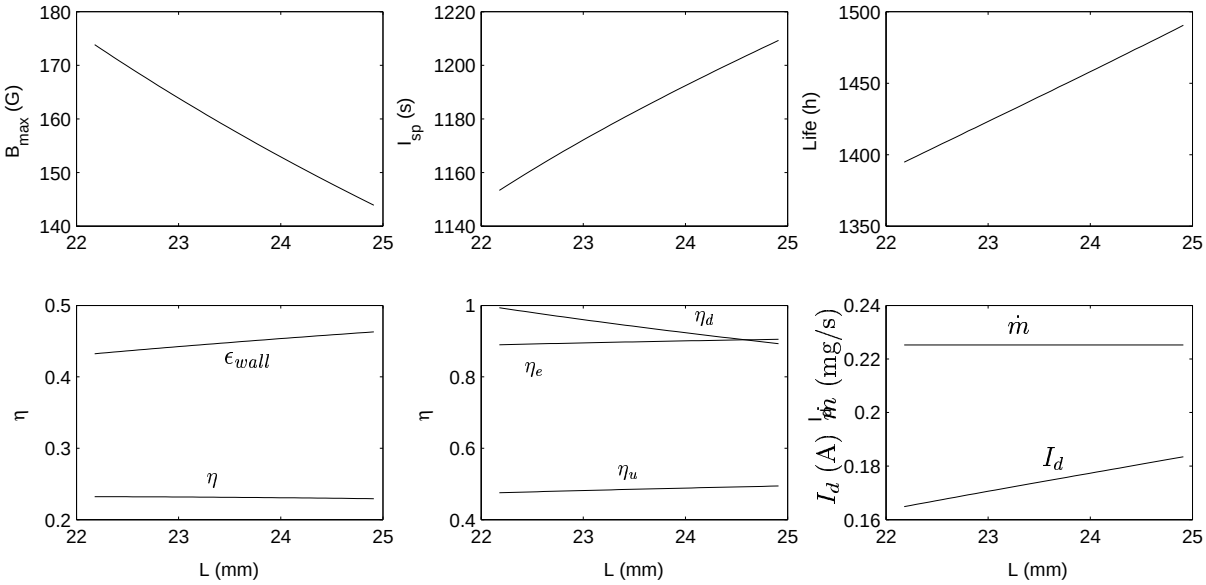

Fig. 4.- Optimization of the efficiency of the mini HT, by modifying the pair (L_c, B_{max}).

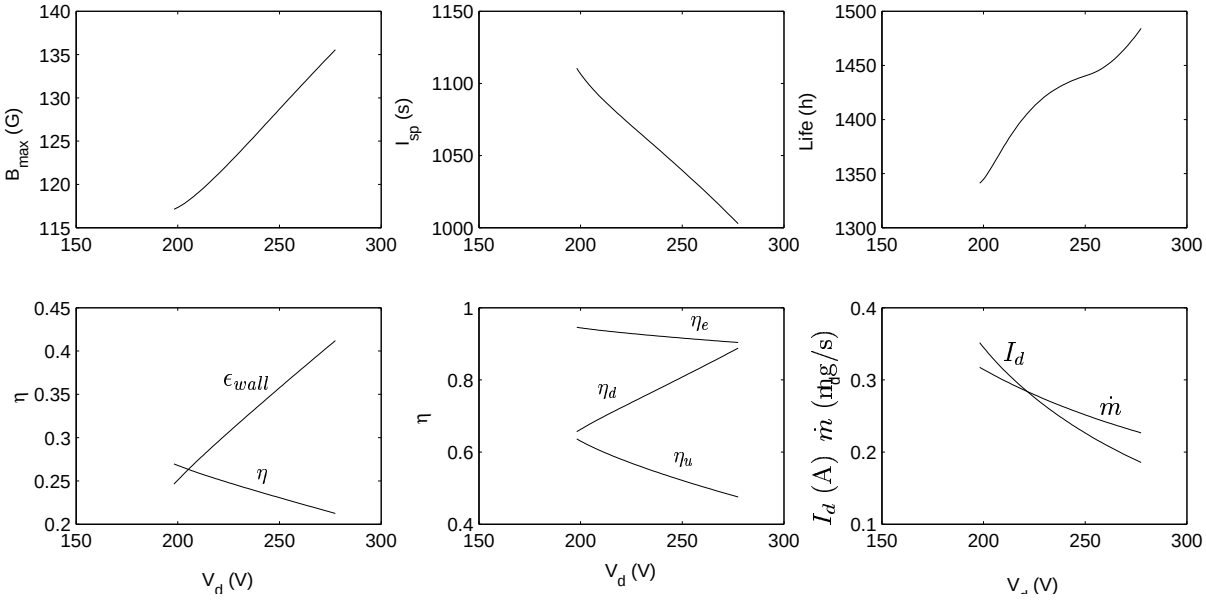

Fig. 5.- Optimization of the efficiency of the mini HT, by modifying the pair V_d and keeping constant the product $V_d \dot{m}_A$.